EVOLUTION IN MOTION: EVIDENCE OF AN ENVIRONMENTAL TRANSITION OF A LOCAL DWARF GALAXY FROM ITS NEUTRAL HYDROGEN STRUCTURE

Luca Beale
Astronomy Department, University of Virginia, Charlottesville, VA 22904

Abstract

Dedicated neutral hydrogen (HI) surveys have recently led to a growing category of exciting low-mass galaxies found in the Local Volume. We present synthesis imaging of one such galaxy, Pisces A, a low-mass dwarf originally confirmed via optical imaging and spectroscopy of HI sources in the Galactic Arecibo L-band Feed Array HI (GALFA-HI) survey. Using HI observations taken with the *Karl G. Jansky* Very Large Array (JVLA), we characterize the kinematic structure of the gas and connect it to the galaxy's environment and evolutionary history. While the galaxy shows overall ordered rotation, a number of kinematic features indicate a disturbed gas morphology. These features are suggestive of a tumultuous recent history and represent $\sim 28\%$ of the total baryonic mass. We find a total baryon fraction $f_{\rm bary} \sim 0.3$ if we include these features. We also quantify the cosmic environment of Pisces A, finding an apparent alignment of the disturbed gas with a local filament. We consider several scenarios for the origin of the disturbed gas. While we cannot rule out stellar feedback from a recent starburst, our observations support the suggestion from previous work that Pisces A has moved from the Local Void to a higher-density filament.

1. Introduction

The survival of gas in dwarf galaxies throughout cosmic history, especially in the low-mass regime, implies that dark matter haloes must shield the gas inside them (e.g., Penny et al., 2009). This relationship is crucial to determining the overall growth of dwarf galaxies, and how their star formation and ISM are coupled (Dekel & Silk, 1986; Kennicutt, 1998; Brooks & Zolotov, 2014). The mechanisms by which dwarfs consume their fuel (and the timescales involved) are complex and poorly studied, especially when HI persists in extended structures around these galaxies (e.g., Roychowdhury et al., 2011).

The cosmic environment of dwarf galaxies can also provide insights into the evolution of their gas content. Low-mass galaxies are thought to accrete their gas mainly through the so-called "cold mode" (Kereš et al., 2005, 2009). The low temperature gas is expected to be transported along cosmic filaments, allowing galaxies to funnel gas from large distances. Possible evidence for such an accretion may be observable in the gas kinematics (possible examples can be found in Stanonik et al., 2009; Kreckel et al., 2011b; Ott et al., 2012). This mechanism is also expected to be more significant in low density regions, and a handful of individual systems from the Void Galaxy Survey (VGS; Kreckel et al., 2014), in which the morphology and kinematics of 59 galaxies selected to reside within the deepest voids identified in the SDSS were studied, reveal kinematic warps and low column density envelopes consistent with gas accretion (see especially Figures 9 and 10 in Kreckel et al., 2012).

Here we present resolved HI imaging of one such low-mass dwarf galaxy taken with the *Karl G. Jansky* Very Large Array (JVLA[1]). Pisces A, a Local Volume dwarf galaxy, was

[1]The National Radio Astronomy Observatory is a facility of the National Science Foundation operated under cooperative agreement by Associated Universities, Inc.

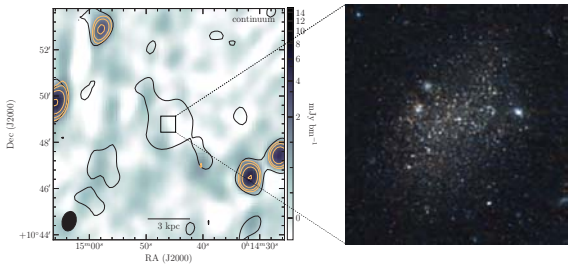

Figure 1 Continuum emission in a $5' \times 5'$ region around Pisces A. Light orange contours highlight continuum sources at the depth of our imaging. The black $2\sigma_{\rm rms} = 56.8$ mJy bm^{-1} $\cdot$ km s^{-1} contour highlighting the extent of the HI emission is from the *foundation*-derived integrated intensity map (see Section 3.1). The $44'' \times 40''$ inset color image shows the optical extent of the galaxy. The colors approximate the human eye response to the F606W/F814W *HST* ACS imaging. See Tollerud et al. (2016) for more details.

originally identified in the GALFA-HI DR1 catalog (Peek et al., 2011) as an HI cloud with a size $< 20'$ and a velocity FWHM < 35 km s^{-1} (Saul et al., 2012; Tollerud et al., 2015). Followup optical spectroscopy (Tollerud et al., 2016) confirmed the coincidence of the HI emission with a stellar component, cementing its status as a galaxy.

From the location of Pisces A within the Local Volume, and its star formation history (SFH), Tollerud et al. (2016) suggest that the galaxy has recently fallen into a higher-density region from a void. If this is indeed the case, the subsequent gas accretion would trigger delayed (recent) evolution and leave an imprint on the gas content observable through the kinematics and morphology. We explore this possibility here by examining the resolved gas kinematics of Pisces A.

This paper is organized as follows: In Section 2, we describe the JVLA observations as well as our techniques for extracting kinematic and morphological information. We highlight the velocity structure and kinematics in Section 3. We place Pisces A in context in Section 4 and conclude in Section 5.

Table 1. Key Parameters of Pisces A

Parameter	Value	Reference
RA (J2000)	$00^{\rm h}14^{\rm m}46^{\rm s}$	
Dec. (J2000)	$+10°48'47.01''$	
Distance (Mpc)	$5.64^{+0.15}_{-0.13}$	(3)
Optical b/a ($= q$)	0.66 ± 0.01	(3)
Inclination (°)	59 ± 9	(1)
$r_{\rm eff,major}$ (pc)	145^{+5}_{-6}	(3)
$\log(M_\star/{\rm M}_\odot)$	$7.0^{+0.4}_{-1.7}$	(3)
$v_{\rm sys,opt}$ (km s^{-1})	240 ± 34	(2)
Arecibo		
$v_{\rm sys,HI}$ (km s^{-1})	236 ± 0.5	(2)
$W50_{\rm HI}$ (km s^{-1})	22.5 ± 1.3	(2)
$M_{\rm HI}$ (10^6 M$_\odot$)	8.9 ± 0.8	(2, 3)
KAT-7 Array		
$v_{\rm sys,HI}$ (km s^{-1})	233 ± 0.5	(4)
$W50_{\rm HI}$ (km s^{-1})	28 ± 3	(4)
$M_{\rm HI}$ (10^6 M$_\odot$)	13 ± 4	(3, 4)
JVLA		
$v_{\rm sys,HI}$ (km s^{-1})	236.0 ± 0.8	(1)
$W50_{\rm HI}$ (km s^{-1})	26 ± 2	(1)
$M_{\rm HI}$ (10^6 M$_\odot$)	7.1 ± 1.6	(1)

(1) This work. (2) Tollerud et al. (2015).
(3) Tollerud et al. (2016). (4) Carignan et al. (2016)

2. Data & Methods

Pisces A was observed in December 2015 with the JVLA in D-configuration for 2h, corresponding to $\sim$ 1.3h of on-source integration time (JVLA/15B-309; PI Donovan Meyer). This is the most compact configuration available for the JVLA, which gives increased sensitivity to extended emission. Observations were centered on the HI line (rest frequency: 1.42040580 GHz) and spanned 8 MHz subdivided into 2048 channels. Standard calibration of the visibility data was done within the Common Astronomy Software Applications (CASA) environment. The calibrated data were then split off into their own MeasurementSet for further analysis. The galaxy is shown in Figure 1 and its parameters are summarized in Table 1.

2.1. Data Cubes

A clean HI data cube is produced by binning to a velocity resolution of 2 km s^{-1} and interac-

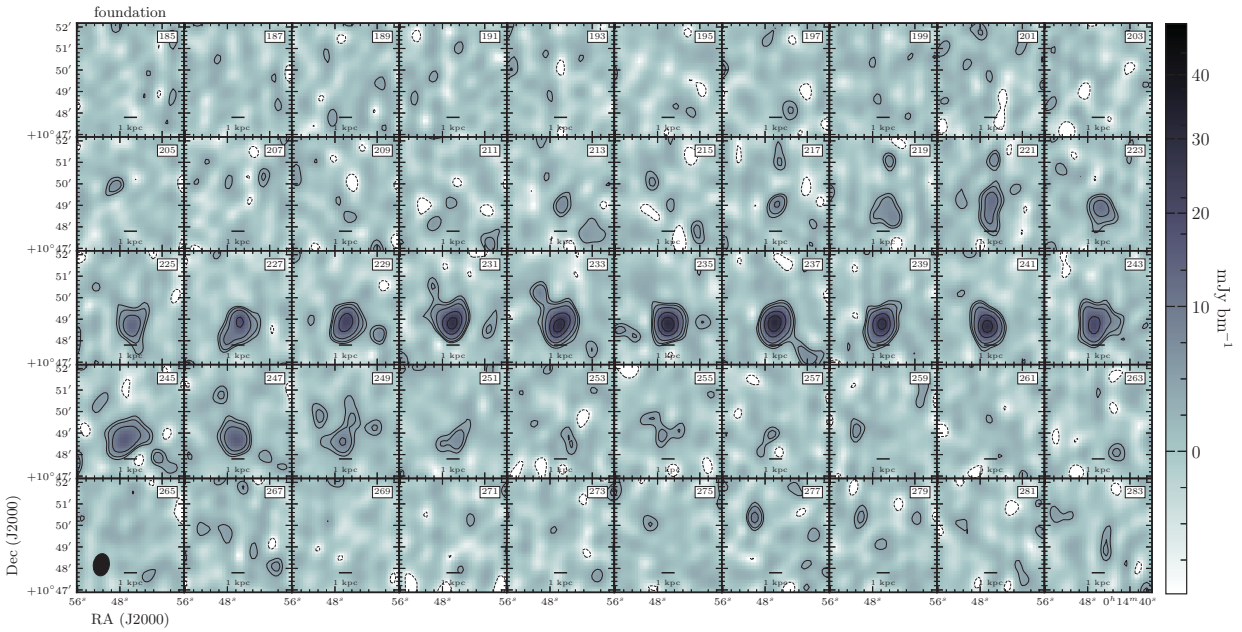

Figure 2 Channel maps from the *foundation* data cube of Pisces A. Contour levels are at (-2, 2, 3, 5, 10, 15)$\sigma_{\rm rms}$ where $\sigma_{\rm rms} = 1.6$ mJy bm^{-1}. The velocity (in km s^{-1}) is marked in the upper right corner of each panel. The JVLA beam is given in the lower left panel.

Table 2. Properties of the Data Cubes

Cube	Δ v (km s^{-1})	Beam ($''\times''$)	$\sigma_{\rm rms}$ (mJy bm^{-1})
foundation	2	62.31×44.68	1.6
narbeam	2	48.57×34.05	2.4
narchan	1	61.81×45.01	1.9
widechan	4	62.24×44.70	1.4

tively masking real emission until the residuals appear noiselike. Imaging is restricted to a 100 km s^{-1} range centered on the systemic HI velocity (Tollerud et al., 2016) as no significant emission is observed outside this region.

To maximize our sensitivity to both small scale structure as well as extended emission, we produce multiple versions of the data cube with different imaging parameters, as summarized in Table 2. In the *narbeam* data cube, we increase spatial resolution by flagging data in the Fourier domain, which in principle increases our sensitivity to the most compact emission. Improved spectral resolution (at the cost of signal-to-noise ratio) in the *narchan* data cube is achieved by binning to 1 km s^{-1} velocity resolution. Finally, the *widechan* data cube is binned to 4 km s^{-1} channels for increased sensitivity to extended structure, at the cost of spectral resolution.

We derive moment maps for Pisces A from the cleaned data cubes using the `immoments` task in CASA. Velocity fields (moment 1) and dispersion maps (moment 2) are clipped to the $\geq 3\sigma_{\rm rms}$ level.

2.2. PV Diagrams

Position-velocity (PV) diagrams are constructed by placing slices across the galaxy and extracting the velocity information at each pixel along the slice, while encompassing the total spatial extent of emission. An approximate "major" axis is defined using the HI isovelocity contours, and an "extension" axis is defined to cross the northeast extension (see Section 3.2). Both axes are centered on the

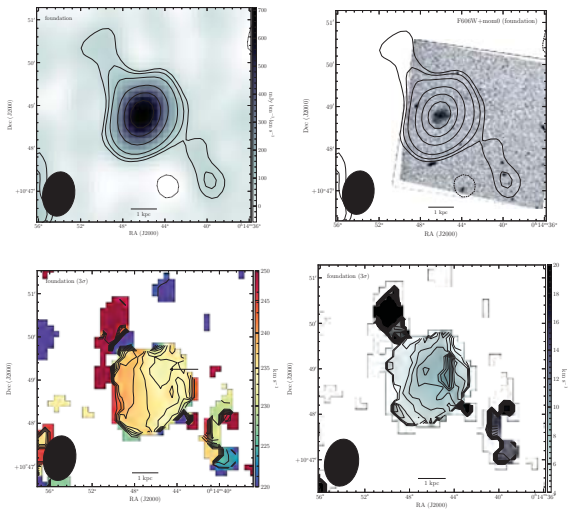

Figure 3 Moment analysis of the *foundation* data cube. The JVLA beam is given in the bottom left corner of each panel. *Top Left*: Integrated intensity map. Contour levels are at (-2, 2, 3, 5, 10, 15, 20)$\sigma_{\rm rms}$ where $\sigma_{\rm rms} = 1.6$ mJy bm^{-1}. *Top Right*: *HST* ACS F606W imaging of Pisces A. Contours are the same as in the top left. *Bottom Left*: Velocity field of the galaxy, as described in Section 2.1. Isovelocity contours are spaced every 2 km s^{-1}, and the thick black contour denotes the systemic velocity. *Bottom Right*: Dispersion map with contours spaced every 2 km s^{-1}.

coordinates of Pisces A as given in Table 1 so that a $0''$ offset corresponds to the optical center of the galaxy.

2.3. Rotation Curves

A full analysis of the rotation curve requires both high spectral and spatial resolution in order to fit the velocity field (typically via tilted-ring models). The extent of the HI in Pisces A ($\sim 2'$ across, corresponding to 2-3x the beam size) prohibits us from taking advantage of this method. Instead, we use a variation of the peak intensity method (Mathewson et al., 1992) to estimate the rotation curve.

From the major-axis PV diagram, we select the pixels with maximum intensity across the spatial direction. After masking to emission at

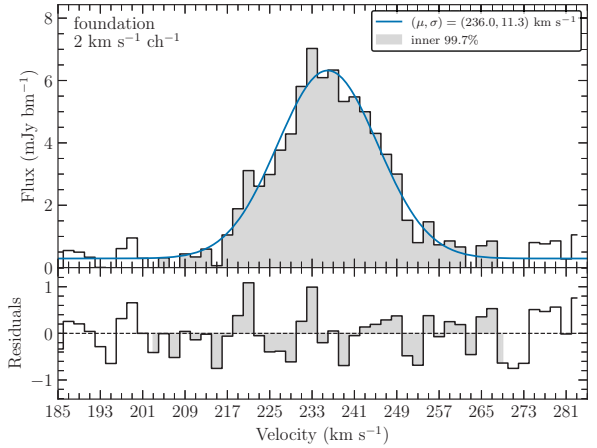

Figure 4 Global HI spectrum extracted from the *foundation* cube. The blue solid curve is the best fit Gaussian. In both panels, the shaded region (containing 99.7% of the emission) denotes the range of emission used in further calculations.

the $\geq 2\sigma_{\rm rms}$ level and removing outlier bright pixels believed not to follow the galaxy rotation, we rebin the data to only sample every half-beam. To estimate the associated uncertainties, we fit a Gaussian to the intensities at each pixel bin, and treat the resulting estimate of $v_{\rm rot}$ as the "true" solution. We then draw random samples from a distribution with the same parameters as the initial solution and re-fit, repeating this 1000 times. The errors are estimated as median$(v_{\rm rot,fit} - v_{\rm rot,true})/2$, added in quadrature with the channel width for that cube.

3. Results

3.1. Overall HI Content and Kinematics

Channel maps for the *foundation* cube are presented in Figure 2. In general, the channel maps reveal regular emission across the main body of the galaxy, which is also seen in other data cubes. However, multiple features are observed which are inconsistent with the general rotation, which we discuss in detail in Section 3.2.

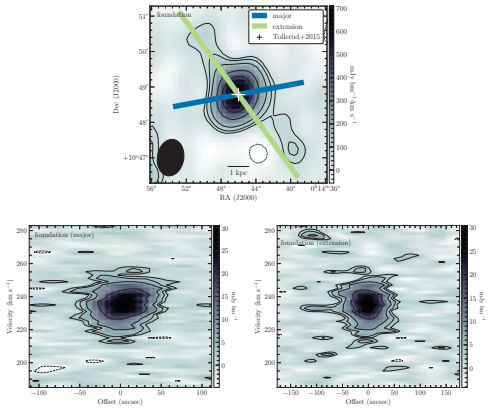

Figure 5 *Top*: Moment 0 map of Pisces A demonstrating the construction of the position velocity slices. Integrated intensity contours are the same as in Figure 3. Also overlaid are the coordinates of the galaxy as given by Tollerud et al. (2015). *Bottom Left* and *Right*: Corresponding major- and extension-axis PV diagrams. Contours are at (-2, 2, 3, 5, 10, 15)$\sigma_{\rm rms}$, where $\sigma_{\rm rms} = 1.6$ mJy bm^{-1}. The northeast extension is approximately near $-100''$ in the extension-axis PV diagram.

In Figure 3 we show the moment analysis for Pisces A, as applied to the *foundation* data cube. The overall HI distribution (top left panel) is centered on the optical component of the galaxy and exhibits extensions toward the northeast and southwest. Both features are also seen in the channel maps, although the southwestern feature is mostly bright in a few noncontiguous channels. These features are discussed further in Section 3.2.

The velocity field of Pisces A is shown in the bottom left panel of Figure 3. Pisces A exhibits approximately solid-body rotation out to the extent of the HI, consistent with typical expectations of dwarf galaxies. There is a slight asymmetry on the approaching side (marked by the arrow in Figure 3), which is approximately at the edge of the optical disk, indicating a possible warp. The dispersion map in the bottom right panel also suggests an approximately rotation-dominated body. We stress that although both maps only include emission $\geq 3\sigma_{\rm rms}$, there may still be unphysical features present, which can be especially seen in the velocity field.

The global HI spectrum of the galaxy is presented in Figure 4. We find a systemic velocity of $v_{\rm sys,HI} = 236.0 \pm 0.8$ km s^{-1}, in agreement with previous single dish and compact array observations. The 50% profile width (uncorrected for inclination or broadening) is $W50_{\rm HI} = 26 \pm 2$ km s^{-1}. We also find an HI mass of $M_{\rm HI} = (7.1 \pm 1.6) \times 10^6$ M$_\odot$.

PV diagrams for Pisces A are shown in Figure 5, along with an integrated intensity map demonstrating the selection process. The overall rotation appears shallow, with the faintest contours contributing little to the bulk motion. In both the major- and extension-axis PV diagrams, we observe fragmented emission at multiple velocities and spatial offsets, which we next discuss in turn.

3.2. Beyond Bulk Motion

The Northeast Extension

One of the most striking features we detect is a 'filament' of gas extending toward the northeast. We call this the "northeast extension" (NEe) when referring to *all* spatially coincident emission in this region. In Figure 2, it is most visible across a few channels near 233 km s^{-1}, but it also appears in the moment maps (Figure 3), and the extension-axis PV diagram in Figure 5 suggests that there are multiple kinematically distinct features in that region.

To assess the significance of the brightest components, we extract a global spectrum of the NEe which we show in the right panels of Figure 6. In the *narbeam* cube, we observe three kinematically distinct components at 227 km s^{-1}, 243 km s^{-1}, and 277 km s^{-1}, which we label as NElow, NEmid, and NEhigh, respectively. Per channel estimates of the rms noise and peak intensity suggest all three components are detected at the $> 3\sigma_{\rm rms}$ level, and all have approximately Gaussian profiles.

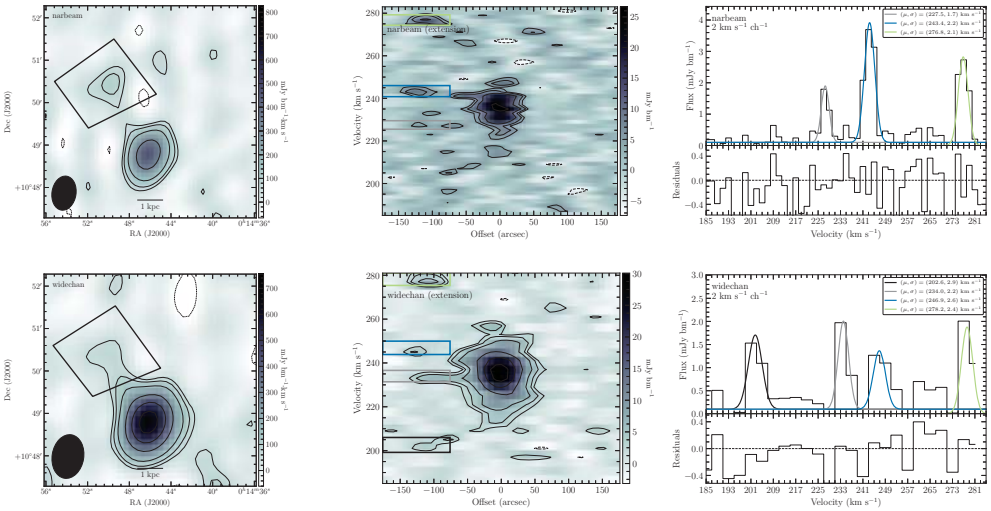

Figure 6 Kinematic decomposition of the NEe in the *narbeam* (top) and *widechan* (bottom) data cubes. *Left*: Selection process based on moment 0 maps. The black trapezium outlines the region used to extract the global spectrum. Contours are at (-2, 2, 3, 5, 10)$\sigma_{\rm rms}$, where $\sigma_{\rm rms} = 2.4$ (1.4) mJy bm^{-1} for the *narbeam* (*widechan*) cube. *Center*: Extension-axis PV diagram with contours similar to Figure 5. The colored rectangles bound the spatial and spectral extent of the best fit Gaussians. *Right*: Corresponding global spectrum of the NEe. Thick colored lines represent Gaussian fits to the brightest components. Colors are the same as the rectangles in the center panels.

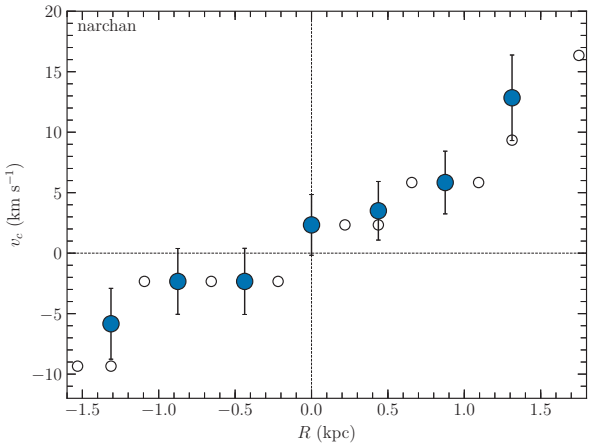

Figure 7 Rotation curve of Pisces A from the *narchan* data cube. Open circles denote the $> 2\sigma_{\rm rms}$ oversampled pixels. The final resampled rotation curve is marked by the blue filled circles. Negative galactocentric distances indicate the approaching side.

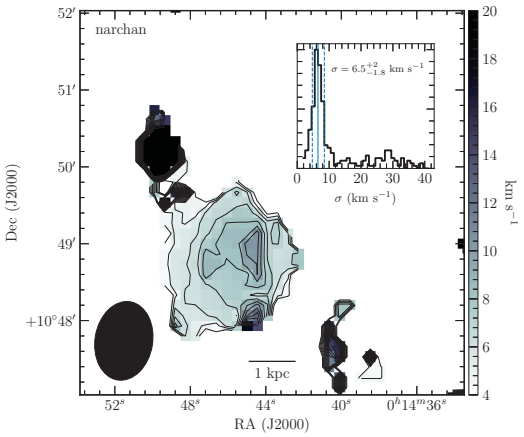

Figure 8 Dispersion map from the *narchan* data cube. Contours are spaced at 1 km s^{-1} intervals. *Inset*: Corresponding distribution of velocity dispersions. The NEe is visible at ~ 28 km s^{-1}.

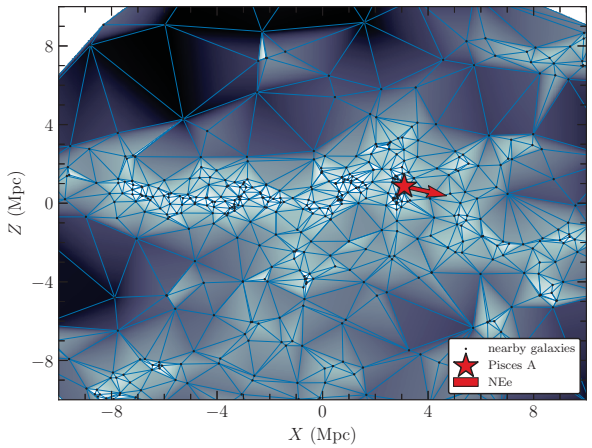

Figure 9 The cosmic density field around Pisces A. Black points are a sample of nearby galaxies (following the prescription in Tollerud et al., 2016). Pisces A is shown as a red star. The Delaunay triangulation is given in blue, with the corresponding density field in greyscale. In this coordinate system, the Z-axis is pointed toward the Local Void.

A similar analysis of the NEe with the *widechan* data cube also reveals multiple distinct components, but at slightly different velocities and signal-to-noise ratios (SNRs). Here, the NEe is most significant at $\sim$ 233 km s^{-1} (corresponding approximately to NElow), similar to what is seen in the *foundation* cube. The disagreement in spectral location may indicate that the most compact emission exists at lower velocities (to which the *narbeam* cube would be most sensitive), while fainter emission (which the *widechan* cube could detect) is at higher velocities.

The Southwest Emission

The moment analysis presented in Figure 3 reveals a peanut-shaped feature which we refer to as the "southwest emission" (SWe). This feature, which appears aligned with the NEe, is detected in all data cubes except for *narbeam* (see the top left panel of Figure 6), suggesting that it is mostly diffuse gas. We perform a similar kinematical decomposition for this feature. It persists across multiple channels, and the peak intensity is detected at the $3\sigma_{\rm rms}$ level.

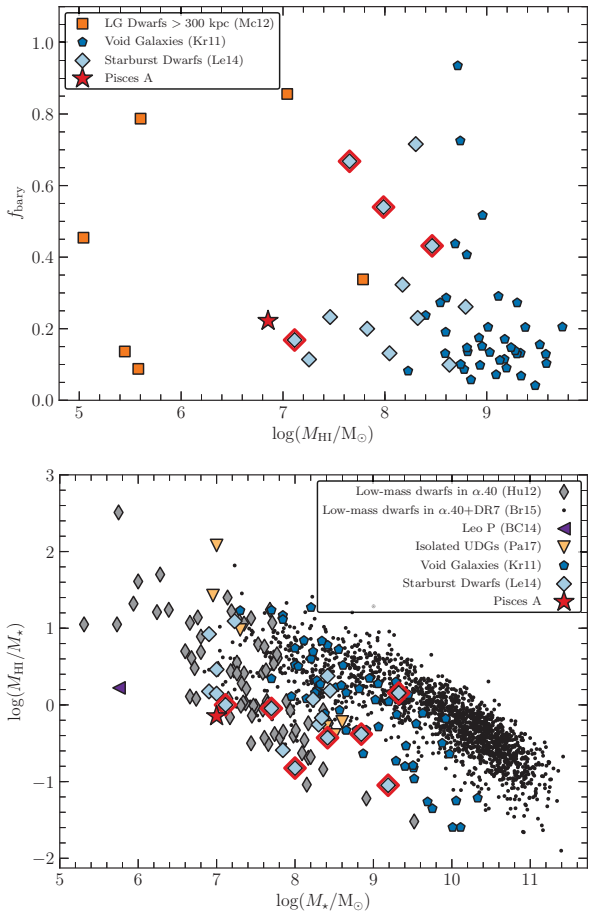

Figure 10 *Top*: The $\log M_{\rm HI} - f_{\rm bary}$ plane. Pisces A is plotted as a red star. *Bottom*: The $\log M_\star - \log(M_{\rm HI}/M_\star)$ plane. See text for description of all samples.

The Northern Clump

A small feature appears in the channel map (Figure 2) at 219 km s^{-1} approximately 2′ above Pisces A, which we dub the "northern clump" (NC). Recurring across multiple channels at the $3\sigma_{\rm rms}$ level, it appears to be separated from the main body of the galaxy. However, the shape of Pisces A at 221 km s^{-1} suggests a possible spatial connection.

Table 3 summarizes the HI properties of all anomalous HI features. We indicate which data cube is used to calculate all parameters in parentheses. Separations are calculated with respect to the optical center of Pisces A, and both separations and sizes assume the clump is

Table 3. Derived HI Clump Properties

	(*narchan*)		
Parameter	SWe	NC	
$v_{\rm fit}$ (km s^{-1})	213.1 ± 0.6	219.2 ± 0.8	
$v_{\rm peak}$ (km s^{-1})[a]	214	220	
Separation (kpc)[b]	3.0	3.8	
Size (kpc)[b,c]	1.5	1.1	
$\Delta v_{\rm fit}$ (km s^{-1})[e]	-22.9 ± 1.0	-16.8 ± 1.1	
$\Delta v_{\rm peak}$ (km s^{-1})[e]	-22	-16	
$W50_{\rm HI}$ (km s^{-1})	5.9 ± 1.9	5.5 ± 2.2	
$M_{\rm HI}$ (10^5 M$_\odot$)	5.9 ± 1.4	2.6 ± 1.3	
	(*narbeam*)		
	NElow	NEmid	NEhigh
$v_{\rm fit}$ (km s^{-1})	228 ± 1	243.4 ± 0.3	276.8 ± 0.3
$v_{\rm peak}$ (km s^{-1})[a]	233	243	277
Separation (kpc)[b]	2.8	2.5	3.0
Size (kpc)[b,d]	1.5	1.1	1.7
$\Delta v_{\rm fit}$ (km s^{-1})[e]	-8.5 ± 1.3	7.4 ± 0.9	40.8 ± 0.8
$\Delta v_{\rm peak}$ (km s^{-1})[e]	-3	7	41
$W50_{\rm HI}$ (km s^{-1})	3.9 ± 3.0	5.2 ± 1.0	4.9 ± 0.7
$M_{\rm HI}$ (10^5 M$_\odot$)	6.3 ± 2.6	15.7 ± 3.1	9.0 ± 3.1

[a] Channel of brightest emission.
[b] Measured in the $v_{\rm peak}$ channel.
[c] Based on the $2\sigma_{\rm rms}$ contour.
[d] Based on the $3\sigma_{\rm rms}$ contour.
[e] Defined as $v - v_{\rm sys,HI}$ (see Table 1).

at the same distance as the galaxy itself.

3.4. Dynamics & Baryon Fraction

In Figure 7 we present the rotation curve of Pisces A, derived from the *narchan* data cube in order to best characterize the rotation. It is clear that the rotation curve is still rising out to the last measured data point, indicating that we are only detecting the solid body rotation of the galaxy. This is expected considering the beam size relative to Pisces A.

Because we do not have a complete knowledge of the matter distribution in the galaxy, i.e., the detailed interplay between rotation and dispersion, we do not have a direct method of calculating the total dynamical mass. Instead, we use the following approximation:

$$M_{\rm dyn} = 2.325{\times}10^5\,{\rm M}_\odot \left(\frac{v_{\rm rot}^2 + 3\sigma^2}{\rm km^2\ s^{-2}}\right)\left(\frac{R}{\rm kpc}\right), \quad (1)$$

where $v_{\rm rot}$ is the rotational velocity, σ is the velocity dispersion, and R is the galactocentric distance. This functional form gives weight to both the rotation and dispersion components in dwarf galaxies (see Hoffman et al., 1996, and references therein).

Figure 8 shows the dispersion map and corresponding distribution of values, also derived from *narchan*. Note that the distribution includes the NEe (the small bump near ~ 28 km s^{-1}), but excludes the SWe. We find a velocity dispersion of $\sigma = 6.5^{+2}_{-1.8}$ km s^{-1}, where the errors represent the inner 68% of the values.

Assuming $v_{\rm rot} = 12.8$ km s^{-1} and $R = 1.3$ kpc from Figure 7, we find a total dynamical mass of $M_{\rm dyn} = (9.0 \pm 3.6) \times 10^7$ M$_\odot$. It is important to stress that this is a lower limit, since we have not captured the full rotation curve. Additionally, the effects of smoothing act to flatten the rotation curve, further underestimating $v_{\rm rot}$. Assuming the total baryonic mass is $M_{\rm bary} = M_\star + 1.4 M_{\rm HI}$ (for a discussion of the factor of 1.4, see McGaugh, 2012), we find a baryon fraction of $f_{\rm bary} = \frac{M_{\rm bary}}{M_{\rm dyn}} = 0.22 \pm 0.28$. Note that we exclude the HI clumps (discussed in Section 3.2) from the total baryonic mass. Including these in the baryonic mass budget raises $f_{\rm bary}$ by $\sim 28\%$ to $f_{\rm bary} = 0.28 \pm 0.29$.

4. Pisces A in Context

4.1. Cosmic Environment

Tollerud et al. (2016) highlighted the fact that Pisces A appears to lie near the boundary of local filamentary structure. Using a sample of galaxies within the Local Volume (see their Section 6 for a full discussion of the data), they showed that Pisces A is located in an overdensity, and that the overdensity points toward the Local Void (18^h38^m 18°; Karachentsev et al., 2002).

We investigate this idea further by characterizing the underlying density field. We employ the basic method of Sousbie (2011), which takes advantage of the fact that the structures of the cosmic web (voids, walls, filaments) have

well-defined analogues in computational topology. A full description of this method is beyond the scope of this paper, but we summarize it as follows: given the positions and distances of some catalog of galaxies, we can construct the Delaunay triangulation (and thus, the underling density field) by assuming the locations of the galaxies accurately sample the local density. We refer the reader to Sousbie (2011) and references therein for a more complete description.

The Delaunay triangulation of galaxies in the Local Void (and the estimated underlying density field) is presented in Figure 9. As this is a simplified version of the method of Sousbie (2011), our reconstructed cosmic web has artificially sharp boundaries, and has not been smoothed to eliminate noise spikes. However, it is immediately clear that there is filamentary structure in the underlying density field, beyond the appearance of the data themselves. Pisces A is well within this filament, supporting the idea of its current membership. Additionally, the NEe appears to be roughly parallel to the filament, which is also observed in other coordinate plane projections.

4.2. The Dwarf Galaxy Population

In Figure 10, we place Pisces A in the $\log M_{\rm HI} - f_{\rm bary}$ plane. Also plotted are a sample of Local Group galaxies from McConnachie (2012, orange squares), galaxies from the Void Galaxy Survey (blue pentagons; Kreckel et al., 2011a, 2014), and a sample of nearby starburst dwarf galaxies (light blue diamonds; Lelli et al., 2014b). Note that starburst galaxies marked has having kinematically disturbed HI disks (outlined in red) do not have reliable rotation curves – instead, the kinematical parameters are estimated from the outermost parts. Pisces A has a baryon fraction broadly similar to both the void galaxy population and the local starburst dwarf population.

Figure 10 also shows the HI mass fraction as a function of the stellar mass. For context, we include low-mass dwarfs in the ALFALFA catalog (grey thin diamonds and small black dots; Giovanelli et al., 2013; Huang et al., 2012; Bradford et al., 2015), Leo P (purple triangle; Bernstein-Cooper et al., 2014), isolated ultra-faint dwarfs (yellow triangles; Papastergis et al., 2017), as well as the void galaxies and starburst dwarfs previously described. While Pisces A is similar to other low-mass dwarfs observed by ALFALFA, it is somewhat gas-poor for its stellar mass, with an HI fraction of $\log\left(M_{\rm HI}/M_\star\right) < 0$. However, including the HI clumps yields an HI mass of $M_{\rm HI,tot} \sim 1.1\times10^7$ $M_\odot$, making it somewhat gas-rich.

5. Discussion and Conclusions

The variety of spatially and kinematically distinct components in the HI distribution of Pisces A suggests that it is not yet in equilibrium. In particular, our results in Table 3 suggest that there exist relatively large clumps (up to 50% of the extent of Pisces A itself) harboring almost 10% of the gas mass as in the main body of the galaxy.

It is difficult to explain the origin of these clumps. One possibility is that they are markers of past mergers. Recent interactions or mergers with other dwarf galaxies have been invoked as possible triggers for recent star formation (e.g., Noeske et al., 2001). Nidever et al. (2013), in particular, detected a long gas extension associated with the nearby starburst galaxy IC 10. They argue that this feature is most likely the result of a recent interaction or merger, and that the interaction also triggered a recent (< 10 Myr) starburst.

Nidever et al. (2013) explicitly rule out a stellar feedback origin to the extension in IC 10 since this would require outflow velocities ~ 30 times the observed velocity offset. However, stellar feedback is not ruled out as an origin for the NEe. The SFH of Pisces A implies increased star formation within 300 Myr (Tollerud et al., 2016). Assuming the furthest observed extent (3.5 kpc, measured from

NEmid), this would imply feedback-driven outflow velocities of $3.5\ \mathrm{kpc}/300\ \mathrm{Myr} \approx 11.7\ \mathrm{km\ s^{-1}}$, slightly larger, but still comparable, to the observed offset of 7.4 km s^{-1}. Pisces A is broadly similar to other local starbursting dwarf galaxies (Lelli et al., 2014a,b), lending further support to this idea.

Interestingly, the NEe approximately points in the direction of the filament, and therefore, is roughly perpendicular to the Local Void. This is what we would expect if Pisces A was accreting gas along filaments via the so-called "cold mode" (Kereš et al., 2005), and this may explain the negative velocity offset of NElow.

In summary:

- With the resolution afforded by the JVLA, we detect multiple morphological and kinematic features in the HI distribution not previously observed. These features are indicative of non-equilibrium, and suggest an active history.

- By further quantifying the environment in which Pisces A resides, we confirm its existence within a cosmic filament. Our observations provide strong support to the idea that the galaxy has recently transitioned from a relatively under-dense environment to an over-dense environment.

Acknowledgments

This work was partially supported by the National Radio Astronomy Observatory and the Virginia Space Grant Consortium under grant NNX15A120H. This research made use of NASA's ADS Bibliographic Services.

References

Bernstein-Cooper, E. Z. et al. 2014, AJ, 148, 35
Bradford, J. D. et al. 2015, ApJ, 809, 14
Brooks, A. M. et al. 2014, ApJ, 786, 87
Bullock, J. S. et al. 2017, ARA&A, 55, 343
Carignan, C. et al. 2016, A&A, 587, L3
Dekel, A. et al. 1986, ApJ, 303, 39
Giovanelli, R. et al. 2013, AJ, 146, 15
Grcevich, J. et al. 2009, ApJ, 696, 385
Hoffman, G. L. et al. 1996, ApJS, 105, 269
Huang, S. et al. 2012, ApJ, 756, 113
Karachentsev, I. D. et al. 2002, A&A, 389, 812
Kennicutt, Jr., R. C. 1998, ApJ, 498, 541
Kereš, D. et al. 2009, MNRAS, 395, 160
Kereš D. et al. 2005, MNRAS, 363, 2
Klypin, A. et al. 1999, ApJ, 522, 82
Kreckel, K. et al. 2011a, AJ, 141, 204
Kreckel, K. et al. 2011b, AJ, 141, 4
Kreckel, K. et al. 2012, AJ, 144, 16
Kreckel, K. et al. 2014, ArXiv e-prints, arXiv:1410.6597
Lelli, F. et al. 2014a, A&A, 566, A71
Lelli, F. et al. 2014b, MNRAS, 445, 1694
Mathewson, D. S. et al. 1992, ApJS, 81, 413
McConnachie, A. W. 2012, AJ, 144, 4
McGaugh, S. S. 2012, AJ, 143, 40
Nidever, D. L. et al. 2013, ApJL, 779, L15
Noeske, K. G. et al. 2001, A&A, 371, 806
Ott, J. et al. 2012, AJ, 144, 123
Papastergis, E. et al. 2017, A&A, 601, L10
Peek, J. E. G. et al. 2011, ApJS, 194, 20
Penny, S. J. et al. 2009, Astron. Nach., 330, 991
Roychowdhury, S. et al. 2011, MNRAS, 414, L5
Saul, D. R. et al. 2012, ApJ, 758, 44
Sousbie, T. 2011, MNRAS, 414, 350
Stanonik et al. 2009, ApJL, 696, L6
Tollerud, E. J. et al. 2015, ApJL, 798, L21
Tollerud, E. J. et al. 2016, ApJ, 827, 89